

Pulsed cavity ring-down spectrometer at 3 μm based on difference frequency generation for high-sensitivity CH_4 detection

C. Bahrini¹ · Y. Bénilan¹ · A. Jolly¹ · B. Lebert¹ · X. Landsheere¹ · M.-C. Gazeau¹

Received: 11 March 2015 / Accepted: 2 November 2015 / Published online: 23 November 2015
© Springer-Verlag Berlin Heidelberg 2015

Abstract We present a mid-infrared pulsed cavity ring-down spectroscopy (CRDS) setup based on difference frequency mixing of a tunable dye laser pumped by a Nd:YAG laser and the residual 1064 nm pulse in a temperature-stabilized lithium niobate (LiNbO_3) crystal. The performances of such a spectrometer have been investigated by studying the absorption spectrum of methane around 3 μm at room temperature. Our results show a minimum detectable absorption coefficient of $5 \times 10^{-8} \text{ cm}^{-1}$. Our approach combines the excellent sensitivity of CRDS with the wide tunable range of difference frequency generation (DFG) with a dye laser. However, the relatively low resolution of this spectrometer prevents the quantification of methane in a wide pressure range. To our knowledge, we report here the first realization and application of a pulsed DFG-based CRDS experiment used for sensitive trace gas detection.

1 Introduction

This work is developed in the context of the SETUP (French acronym for Experimental and Theoretical Simulations Useful for Planetology), a laboratory program which focuses on simulating Titan's atmosphere experimentally [1, 2]. The atmosphere of Titan and mainly its stratosphere is host to an organic-rich chemistry where its principle constituents, nitrogen (98 %) and methane (~1.6 %), are dissociated and react to form larger molecules (mainly

hydrocarbons and nitriles), which can eventually condense into solid organic aerosols. The SETUP program is developed to mimic such mechanisms in the most representative conditions. The coupled N_2/CH_4 chemistry is initiated in a flow reactor using electrons as well as Lyman- α photons. Indeed, both energy sources contribute strongly in the stratospheric region. The vacuum pumping and measurement system allow performing experiments at pressures above 10^{-3} mbar. We set the total pressure of the gas mixture around 1 mbar to simulate Titan's upper stratosphere. The experiment is run at ambient temperature which does not correspond directly with any region; however, the upper stratosphere and above are the closest match. Cryogenically cooled conditions are planned in future simulations. The ability to perform in situ and quantitative analysis is an improvement in our experimental device over other previous Titan's simulation programs [3]. Indeed, only quantitative data can lead to a critical examination of the accuracy of the chemical scheme of the model developed to reproduce the observations from planetary space missions. Consequently, we have chosen to probe in situ (i.e., in the reaction chamber) the chemical composition of the gas sample and its evolution, using cavity ring-down spectroscopy (CRDS). Indeed, this method fulfills the requirements of high selectivity and sensibility to detect the compounds formed at trace amount in the simulations. Due to the large variety of these compounds, a wide tuning range is needed. All compounds, mainly hydrocarbons and nitriles, have fundamental vibrational transitions in the mid-infrared (2.5–5 μm). That is the reason why we have chosen to perform our studies using a tunable light operating in this wavelength region.

Several varieties of laser sources are now available in the mid-infrared (MIR). For example, quantum cascade lasers (QCLs) [4, 5] provide high power (tens to hundreds

✉ C. Bahrini
chiheb.bahrini@lisa.u-pec.fr

¹ L.I.S.A. (Laboratoire Interuniversitaire des Systèmes Atmosphériques), UMR 7583, CNRS, Universités Paris 7 et 12, 61 Avenue du Général de Gaulle, 94010 Créteil Cedex, France

Table 1 Sensitivity and range of different existing systems

References	Tuning range	Laser width	Sensitivity α_{\min} (cm ⁻¹)
This study	3165–3425 nm 2920–3160 cm ⁻¹	0.06 cm ⁻¹	5×10^{-8}
Whittaker et al. [15] (2012) cw DFG CRDS	3345.38–3345.94 nm 2988.7–2989.2 cm ⁻¹	>10 MHz	3×10^{-8}
Stry et al. [13] (2002) cw DFG CRDS	1.7 cm ⁻¹		1×10^{-8}
Grilli et al. [14] (2010) DFG PS–CRDS	>35 cm ⁻¹	<1 MHz	1.4×10^{-7}
Seiter et al. [10] (1999) Pulsed DFG 36-m multi-pass absorption cell	3160–3670 nm	154 MHz	1.1×10^{-7}
Todd et al. [18] Picarro (2002) Pulsed OPO CRDS	6–8 μ m	2 cm ⁻¹	2×10^{-8}
Aniolek et al. [17] (1999) OPG/OPA CRDS	60 cm ⁻¹	≤ 0.08 cm ⁻¹	2×10^{-8}
Zhao et al. [24] (2013) cw-OPO CRDS	3.2–2.4 μ m 3100–4200 cm ⁻¹	~1 MHz	2×10^{-7}

of mW), can be tuned continuously up to 50 nm, and have linewidths up to tens of kHz when stabilized. QCLs can be operated either in pulsed mode at room temperature or in continuous wave (cw) mode at cryogenic temperatures. Recently, cw monomode distributed feedback (DFB) laser diodes have been commercialized [5, 6]. Their output power is ~1 mW beyond 3 μ m with a typical tuning range of 9 nm and linewidths below 3 MHz. An attractive alternative to QCLs and DFB laser diodes is difference frequency generation (DFG). Lasers exploiting this principle are able to perform high-resolution spectroscopy (~MHz) [7, 8], especially when using narrow linewidth diode laser sources [9] and are often coupled to multi-pass cell [10–12].

There are very few examples in the literature of coupling continuous DFG mid-infrared light into a cavity to perform CRDS: the main ones being those reported by Stry et al. [13] in 2002, Grilli et al. [14], Whittaker et al. [15] and De Natale et al. [16]. However, all of these studies used MIR laser sources with a small wavelength tuning range (~10 nm). Grilli et al. [14] used phase-shift CRDS with MIR radiation around 3081 cm⁻¹ produced by DFG of the outputs of two single-mode diode lasers (1583 and 1064 nm) in a periodically poled lithium niobate crystal (PPLN) for spectroscopy measurements. Ethene detection was demonstrated with a minimum absorption coefficient of 1.4×10^{-7} cm⁻¹.

In 1999, Aniolek et al. [17] presented a CRDS based on periodically poled lithium niobate (PPLN) optical parametric oscillator (OPO) with a linewidth lower than 0.08 cm⁻¹. The performance of such a device and its ability to be used in a gas trace sensor have been demonstrated by the recording of a methane spectrum in the 3020 cm⁻¹ region. In 2002, MIT groups and Picarro, Inc. [18] developed a

pulsed mid-infrared CRDS system also based on OPO to detect trace explosives vapor using an in a large tunable wavelength range (6–8 μ m). Nevertheless, its linewidth (2 cm⁻¹) is too large to allow high-resolution spectroscopy.

Table 1 give a summary of existing system compared to our instrument.

In the present work, we developed a DFG-based CRDS spectrometer which mixes the fundamental beam (1064 nm) of a pulsed Nd:YAG laser with a tunable dye laser.

In this paper, the principles of CRDS, experimental device, data acquisition, and data treatment are successively presented in the experimental section. Next, we report the first spectrum of methane recorded in the 3 μ m region with a DFG pulsed cavity ring-down spectrometer. Finally, we determine the minimum detectable absorption coefficient and discuss the sensitivity of our measurements.

2 Experimental

2.1 CRDS method theory

CRDS is a powerful absorption spectroscopy method based on measurement of the time decay of a pulse of light trapped in a high-finesse optical cavity [19]. The major advantages of this technique are insensitivity to light source fluctuations and the long optical pathlength. While reflecting in the cavity, the light intensity decays due to the transmission and scattering losses of the mirrors. An absorbing sample in the cavity increases this decay rate even further, allowing one to measure the absorption of the sample.

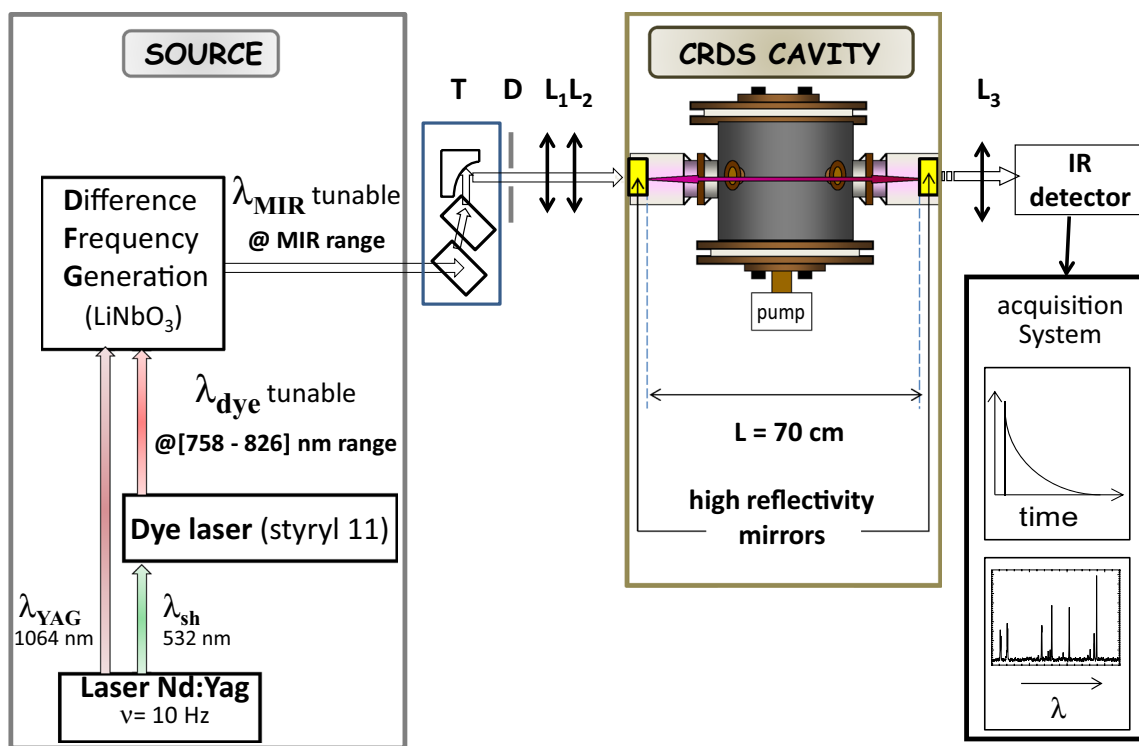


Fig. 1 Experimental device. A Nd:YAG laser (fundamental beam: $\lambda_{YAG} = 1064$ nm and second-harmonic beam: $\lambda_{sh} = 532$ nm), a dye laser (operating with Styryl 11) and a DFG unit (operating with a

LiNbO₃ crystal) are used to provide the tunable MIR beam. *T* telescope, *D* diaphragm, *L*₁, *L*₂ lenses, The CRDS cavity properties are *L* = 70 cm, *R* > 99.7 % (see Sect. 2.3)

The temporal ring-down signal intensity *I*(*t*) may be described by:

$$I(t) = I_0 \int_{-\infty}^{+\infty} d\nu L(\nu - \nu_L) \exp\left(-\frac{t}{\tau(\nu)}\right)$$

$$\Rightarrow I(t) = I_0 \exp\left(-\frac{tc(1-R)}{l}\right) \times \sum_i L_i(\nu_i - \nu_L) \exp\left(-\frac{tcN\sigma(\nu_i)l_{abs}}{l}\right)$$

(1)

where *R* is the mirror reflectivity, *l* the distance between the two mirrors, *l_{abs}* the absorbing length, and *c* the speed of light. The ratio *l/l_{abs}* is equal to 1 in our experiment. *L*(*ν*) the laser profile centered at wavenumber *ν_L*. The ring-down signal represents a sum of exponentials with different decay rates, corresponding to different frequencies, weighted by the laser profile. The exponential factor in front of the summation represents the empty cavity decay, assumed to have no spectral dependence: $\tau_0 = l/c(1-R)$.

If the laser's linewidth is very narrow with respect to the absorption feature width, the laser's profile can be approximated by a Dirac delta function. In this case, the multi-exponential expression (1) reduced to a single exponential with a decay time:

$$\frac{1}{\tau} = \frac{1}{\tau_0} + c\alpha$$

(2)

The absorption coefficient α can be determined from ring-down time τ and τ_0 measured respectively with and without the presence of absorbing species. Knowing the absorption cross section σ , the concentration *N* is then deduced as $\alpha = N\sigma$.

The minimum detectable absorption coefficient, α_{min} , equals $\Delta\tau_{min}/c\tau^2$, where $\Delta\tau_{min}$ is the minimum change in ring-down time that can be measured.

2.2 Laser system

A schematic overview of the experimental apparatus is shown in Fig. 1. A dye laser (Cobra-Stretch dye laser, Sirah Lasertechnik GmbH) is pumped at 532 nm by a frequency-doubled Nd:YAG laser pulsed at 10 Hz (Quanta-Ray Lab 170-Injection Seeded Spectra physics). The current holographic grating is of 90 mm length, 2400 lines/mm. Adding a second grating in the resonator of the dye laser could improve the resolution by a factor two. The dye laser output beam (maximum energy ≈ 25 mJ/pulse) and the residual 1064 nm beam from the Nd:YAG laser are mixed in a temperature-stabilized LiNbO₃ crystal which produces a beam at the difference of their frequencies. The maximum output energies of the fundamental (at 1064 nm) and the second harmonic (at 532 nm) are 980 and 560 mJ, respectively. A

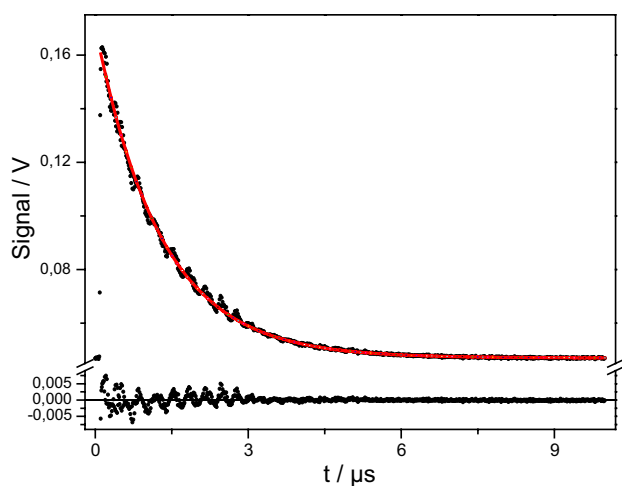


Fig. 2 Example of a ring-down signal at 3067.8 nm averaged over 25 ring-down times. The raw data (*black curve*) were fitted with a single exponential decay (*solid red line*) and the residuals between the data and fit is shown on the *lower plot*. Here, $\tau_0 = (1.279 \pm 0.004) \mu\text{s}$ (1σ)

set of dichroic mirrors separates the generated MIR pulse from the two incoming beams. The organic dye used, Styryl 11 (Sirah Lasertechnik GmbH), emits within a range of 758–826 nm with a maximum at 785 nm. The MIR beam has a spectral width of the order of 0.06 cm^{-1} and a temporal full width at half maximum (FWHM) of 10 ns with 10 Hz repetition rate. The MIR beam's measured energy is 0.8 mJ/pulse. A telescope, a diaphragm, and two lenses L_1 and L_2 (with focal length 25.4 and 500 mm, respectively) are used to couple MIR beam into the ring-down cavity. The optics and diaphragm reduce the energy reaching the cavity from 0.8 to 0.4 mJ/pulse.

2.3 Ring-down cavity

The stainless steel cylindrical chamber (outer diameter 28 cm, length 20 cm) is pumped by a rotary pump and equipped with MKS Baratron manometer for absolute pressure measurements. The high reflectivity mirrors of the cavity are mounted 70 cm from each other, corresponding to a free spectral range of 214 MHz ($7 \times 10^{-3} \text{ cm}^{-1}$). In our case, the laser's linewidth covers approximately 10 discrete free spectral ranges. We use dielectric concave mirrors (Layertec #106548) with a quoted reflectivity $>99.7\%$ between 3.0 and 3.5 μm ($2850\text{--}3300 \text{ cm}^{-1}$). Their radius of curvature is $r = 50 \text{ cm}$, which fulfills the geometric conditions of optical cavity stability ($0 < (1 - L/r)^2 < 1$). Proper cavity alignment, the use of the diaphragm and two lenses are necessary to excite only the lowest order transverse fundamental cavity modes. Indeed the excitation of higher-order transverse modes inside the cavity causes distortion in the exponential decay, particularly oscillations (Fig. 2).

2.4 Detection and data acquisition

As the energy of the transmitted radiation through the cavity is expected to be $<3 \text{ nJ/pulse}$, we use a two-stage thermoelectrically cooled mercury cadmium telluride HgCdZnTe photovoltaic detector (Vigo System, Model PVI-2TE-3.4) with a sensitivity of 89 kV/W at 3.4 μm , and a normalized detectivity of $7.5 \times 10^{11} \text{ cm Hz}^{1/2} \text{ W}^{-1}$. The 10–90 % rise time of the detector is 45 ns. The detector signal is connected to an 8-bit high-speed digitizer (PCI-5112, National Instruments), which is triggered by the Q-switch of the Nd:YAG laser. The digitizer card has a 100 MS/s sampling frequency and thus the ring-down signal is sampled every 10 ns. This approach allows obtaining clean and reproducible exponential decays. The ring-down time is obtained by fitting the decay over 10 μs with a Levenberg–Marquardt exponential fit.

The ring-down signal of an empty cavity at 3259.7 cm^{-1} shown in Fig. 2, comes from the average over 25 individual ring-down events. The number of ring-down times has been optimized to obtain a best signal-to-noise ratio and minimum residuals between the data and fit (Fig. 2). We observed that for more than 25 events the signal-to-noise ratio is almost constant.

In this case the decay time is $\tau_0 = 1.279 \mu\text{s}$, the 1σ -uncertainty $\Delta\tau_0/\tau_0$ is 0.3 %, corresponding to a minimum detectable absorption coefficient of $\approx 7.5 \times 10^{-8} \text{ cm}^{-1}$. The maximum ring-down time of our empty cavity is around 1.7 μs , implying a mirror reflectivity of $\approx 99.86\%$. Therefore, our ring-down cavity has a maximum effective optical absorption path length of the order of 500 m and a minimum detectable absorption coefficient of $\approx 5 \times 10^{-8} \text{ cm}^{-1}$.

3 Results and discussion

3.1 Cavity ring-down spectra of CH_4

A mixture of methane and nitrogen was prepared at a ratio of 1:1000 and connected to the CRDS chamber. The absorption spectrum of methane at room temperature and total pressure of 0.8 Torr ($[\text{CH}_4] = 2.5 \times 10^{13} \text{ cm}^{-3}$) has been recorded in the range 2920–3160 cm^{-1} with a sampling of $1.6 \times 10^{-2} \text{ cm}^{-1}$. The experimental absorption coefficient α shown in Fig. 3 is in good agreement with our simulation based on the HITRAN linelist [20]. This simulation uses a Voigt profile taking into account the sample pressure and the Doppler broadening. We introduce the spectral width of the laser and assume a Gaussian profile with a FWHM of 0.06 cm^{-1} , as discussed in Sect. 2.2. This is 10 times broader than the typical Doppler linewidth in our conditions. The convolution of absorption spectra is

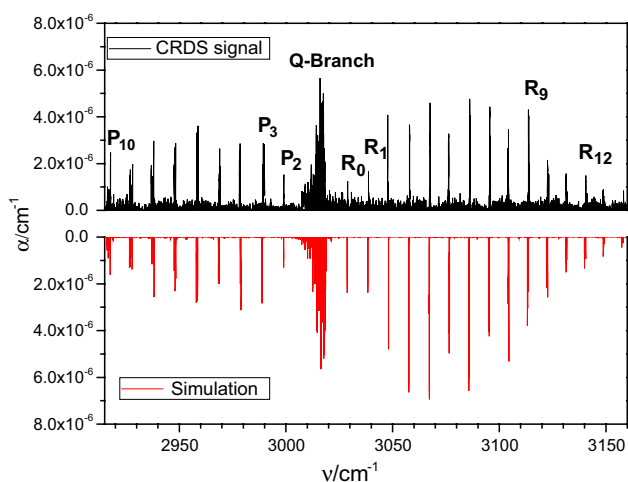


Fig. 3 Overview of the absorption spectrum of the ν_3 band of CH_4 near 3000 cm^{-1} ($\sim 3.3\ \mu\text{m}$). The total pressure was 0.8 Torr. *Upper trace* measured CRDS spectrum. *Lower trace* simulation based on the HITRAN2012 database [20]

nonlinear and experimental saturated spectra can be reasonably well reproduced. Since saturation is very sensitive to the apparatus function as well as line profiles, width and overlap, large differences can be observed for different lines. Those differences are difficult to reproduce with the approximate line and apparatus profiles used in our model.

3.2 Absorption coefficient and pressure dependence

The measured ring-down time τ as a function of wavenumber for the $P(3)$ transition of the fundamental ν_3 band of CH_4 is presented at different total pressures in Fig. 4. Studies were carried out between 0.13 and 4.3 Torr total pressure corresponding to methane density of, respectively, 3.2×10^{12} and $1.1 \times 10^{14}\text{ cm}^{-3}$. The absorption coefficients have been determined for each pressure using Eq. (2).

The actual laser profile causes a broadening of the absorption lines and an associated reduction in the peak maximum. Consequently, peak-based analysis systematically underestimates absorbance. Thus, integrated absorption coefficients were determined by calculating the areas under the lines. Figure 5 displays the integrated absorption coefficient α_{int} versus methane density for the line centered at $\nu = 2988.93\text{ cm}^{-1}$.

The evolution of α_{int} as a function of methane density seems to be linear for lower densities while for higher values we clearly observe a saturation phenomenon. From the linear part of the curve, an integrated cross section of methane $\sigma_{\text{int}} = (4.21 \pm 0.14) \times 10^{-21}\text{ cm molec}^{-1}$ can be deduced. This value is very low compared with the reference value $\sigma_{\text{int}} = 6.39 \times 10^{-20}\text{ cm molec}^{-1}$ given by

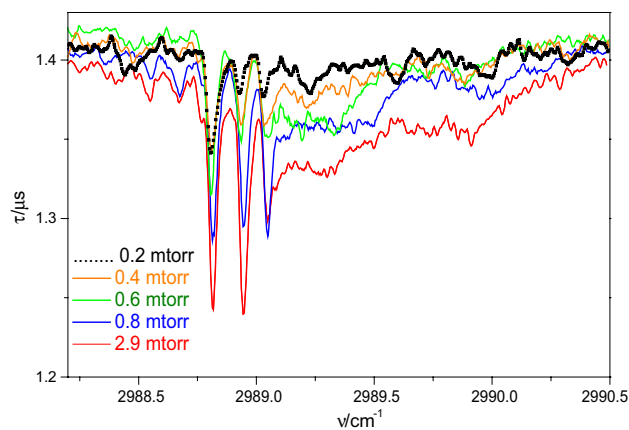


Fig. 4 Ring-down time of $P(3)$ lines versus wavenumber at different CH_4 pressures

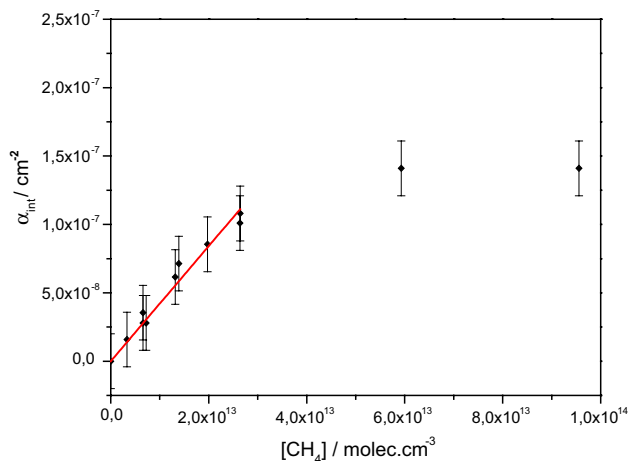


Fig. 5 Integrated absorption coefficient α_{int} versus methane density for the line centered at $\nu = 2988.93\text{ cm}^{-1}$

HITRAN [20]. Qualitatively, the saturation can be reproduced with a standard simulation introducing low or high column density.

3.3 Laser and line-width effects

The advantage of assuming a single exponential is that the ring-down data may be fitted in real time. However, as the laser bandwidth broadens, the single exponential model loses validity [21–23] and for strong absorbers leads to a kind of optical “saturation”.

For the experiments discussed above, we expect a multi-exponential behavior since we used a laser with a FWHM of $\Delta\nu_L \approx 0.06\text{ cm}^{-1}$, which is much larger than the Doppler-broadened CH_4 absorption lines ($\Delta\nu_{\text{Doppler}} \approx 0.0055\text{ cm}^{-1}$).

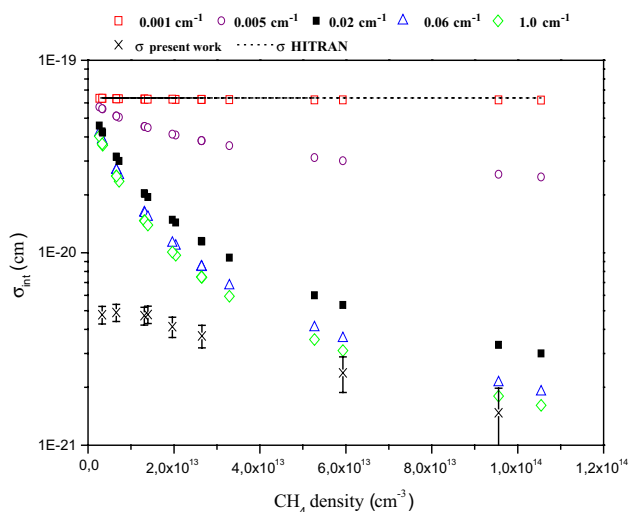


Fig. 6 Simulated integrated cross sections as a function of methane density for different laser widths. The experimental cross sections are also shown (stars)

We simulate the ring-down signal using Eq. (1) and used Hitran line intensities and Voigt profile to reproduce CH_4 absorption cross sections $\sigma(\nu_i)$ in our temperature and pressure conditions. We used a laser profile $L(\nu)$ to simulate the signal $I(t)$. Then, this simulated signal is fitted by a single exponential. Finally, we compare values derived from the fit to the values available in the literature [20].

Figure 6 displays the simulated integrated cross sections at $\nu = 2988.93 \text{ cm}^{-1}$ versus CH_4 density for different laser linewidths. Only narrow laser profiles (0.001 cm^{-1}) would allow retrieving the correct value of σ whatever the density. For larger values of the laser linewidth the simulated values of σ are underestimated especially at high densities. Figure 6 also displays the experimental values of σ measured in this work at 0.06 cm^{-1} . One can observe saturation for high densities as in the simulation. For lower densities, we measured significantly lower values than the simulations. This suggests that we are already saturated at these low densities. This discrepancy could be explained by line mixing which was not included in the simulations. The presence of extra absorption peak nearby is supposed to further reduce the ring-down time constant, and thus reduce the discrepancy between simulation and experimental results. Alternatively, it is also possible that the true laser profile is not perfectly Gaussian.

4 Conclusion and outlook

A pulsed cavity ring-down spectrometer based on difference frequency generation has been developed. We have demonstrated the feasibility of the method and showed that absorption coefficients down to $5 \times 10^{-8} \text{ cm}^{-1}$ are detectable.

Wide spectral tunability has been demonstrated by recording a portion of the absorption spectrum of methane (CH_4) over more than 200 cm^{-1} near $3.2 \mu\text{m}$. The frequency-tuning region can be extended by changing the dye and the crystal (leading to a broad spectral coverage from 3 to $5 \mu\text{m}$) but with a limited spectral resolution. The pulsed DFG CRDS tested in the case of methane could be applied to other systems absorbing in the same spectral range through the C–H stretching vibrational mode around $3 \mu\text{m}$. The CRDS technique has been already used to analyze organic molecules like C_2H_6 [13] at $\sim 3.3 \mu\text{m}$, the ν_9 fundamental C_2H_2 vibrational band [14] at 3081 cm^{-1} , and ro-vibrational transitions of HC_4H and HC_6H [24] around 3330 cm^{-1} .

The broadness of the laser line limits our ability to quantify species density in a large range. However, it would be possible to overcome the problem by a careful choice of the CRDS integration time window. Indeed, Newman et al. [25] and more recently C. Romanzin et al. [26] demonstrated that a quantitative analysis can be derived from the CRDS measurements using a narrow time window for the signal integration at the beginning of the ring-down decay.

Future work includes the development of a cw mid-IR CRDS which provides much better spectral resolution in a narrow spectral range around $3 \mu\text{m}$.

Continuous DFG laser source could be achieved by mixing radiations from two near-IR diode lasers emitting (at 1560 and 1064 nm) in a bulk lithium niobate crystal. Using cw diode lasers technology in the telecommunication range offers many advantages as compactness, cheapness, and narrow linewidths allowing for high-resolution spectroscopy and rapid tunability.

Acknowledgments This work is mainly supported by CNES (Centre National d'Etudes Spatiales) and DIM ACAV Région île de France postdoctoral fellowship.

References

1. C. Romanzin, Y. Benilan, A. Jolly, M.-C. Gazeau, *Adv. Space Res.* **42**, 2036 (2008)
2. C. Romanzin, E. Arzoumanian, E. Es-sebbar, A. Jolly, S. Perrier, M.C. Gazeau, Y. Benilan, *Planet. Space Sci.* **58**, 1748 (2010)
3. M.C. Gazeau, H. Cottin, V. Vuitton, N. Smith, F. Raulin, *Planet. Space Sci.* **48**, 437 (2000)
4. R.F. Curl, F. Capasso, C. Gmachl, A.A. Kosterev, B. McManus, R. Lewicki, M. Pusharsky, G. Wysocki, F.K. Tittel, *Chem. Phys. Lett.* **487**, 1 (2010)
5. W. Zeller, L. Naehle, P. Fuchs, F. Gerschuetz, L. Hildebrandt, J. Koeth, *Sensors* **10**, 2492 (2010)
6. P. Kluczynski, M. Jahjah, L. Nähle, O. Axner, S. Belahsene, M. Fischer, J. Koeth, Y. Rouillard, J. Westberg, A. Vicet, S. Lundqvist, *Appl. Phys. B: Lasers Opt.* **105**, 427 (2011)
7. W. Chen, F. Cazier, D. Boucher, F.K. Tittel, P.B. Davies, *Laser Phys.* **11**, 594 (2001)
8. L. Wang, Z. Cao, H. Wang, H. Zhao, W. Gao, Y. Yuan, W. Chen, W. Zhang, Y. Wang, X. Gao, *Opt. Commun.* **284**, 358 (2011)

9. K.P. Petrov, R.F. Curl, F.K. Tittel, *Appl. Phys. B* **66**, 531 (1998)
10. M. Seiter, M.W. Sigrist, *Opt. Lett.* **24**, 110 (1999)
11. G. Rusciano, G. Pesce, F. Pignatiello, A. Sasso, *Opt. Express* **11**, 3010 (2003)
12. M.W. Sigrist, R. Bartlome, D. Marinov, J.M. Rey, D.E. Vogler, H. Wächter, *Appl. Phys. B* **90**, 289 (2008)
13. S. Stry, P. Hering, M. Mürtz, *Appl. Phys. B* **75**, 297 (2002)
14. R. Grilli, L. Ciaffoni, A.J. Orr-Ewing, *Opt. Lett.* **35**, 1383 (2010)
15. K.E. Whittaker, L. Ciaffoni, G. Hancock, R. Peverall, G.A.D. Ritchie, *Appl. Phys. B* **109**, 333 (2012)
16. P. Cancio, S. Bartalini, S. Borri, I. Galli, G. Gagliardi, G. Giusfredi, P. Maddaloni, P. Malara, D. Mazzotti, P. De Natale, *Appl. Phys. B* **102**, 255 (2011)
17. K.W. Aniolek, P.E. Powers, T.J. Kulp, B.A. Richman, S.E. Bisson, *Chem. Phys. Lett.* **302**, 555 (1999)
18. M.W. Todd, R.A. Provencal, T.G. Owano, B.A. Paldus, A. Kachanov, K.L. Vodopyanov, M. Hunter, S.L. Coy, J.I. Steinfeld, J.T. Arnold, *Appl. Phys. B* **75**, 367 (2002)
19. C. Bahrini, S. Douin, J. Rostas, G. Taïeb, *Chem. Phys. Lett.* **432**, 1 (2006)
20. L.S. Rothman, I.E. Gordon, Y. Babikov, A. Barbe, D. Chris Benner, P.F. Bernath, M. Birk, L. Bizzocchi, V. Boudon, L.R. Brown, A. Campargue, K. Chance, E.A. Cohen, L.H. Coudert, V.M. Devi, B.J. Drouin, A. Fayt, J.-M. Flaud, R.R. Gamache, J.J. Harrison, J.-M. Hartmann, C. Hill, J.T. Hodges, D. Jacquemart, A. Jolly, J. Lamouroux, R.J. LeRoy, G. Li, D.A. Long, O.M. Lyulin, C.J. Mackie, S.T. Massie, S. Mikhailenko, H.S.P. Müller, O.V. Naumenko, A.V. Nikitin, J. Orphal, V. Perevalov, A. Perrin, E.R. Polovtseva, C. Richard, M.A.H. Smith, E. Starikova, K. Sung, S. Tashkun, J. Tennyson, G.C. Toon, V.I. G. Tyuterev, G. Wagner, *JQSRT* **130**, 4 (2013)
21. A.P. Yalin, R.N. Zare, *Laser Phys.* **12**, 1065 (2002)
22. R.T. Jongma, M.G.H. Boogaarts, I. Holleman, G. Meijer, *Rev. Sci. Instrum.* **66**, 2821 (1995)
23. R.D. Van Zee, J.T. Hodges, J.P. Looney, *Appl. Opt.* **38**, 3951 (1999)
24. D. Zhao, J. Guss, A.J. Walsh, H. Linnartz, *Chem. Phys. Lett.* **565**, 132 (2013)
25. S.M. Newman, I.C. Lane, A.J. Orr-Ewing, D.A. Newnham, J. Ballard, *J. Chem. Phys.* **110**, 10749 (1999)
26. C. Romanzin, B. Gans, S. Douin, S. Boyé-Péronne, D. Gauyacq, *Chem. Phys.* **351**, 77 (2008)